JOURNAL OF CATALYSIS **174,** 164–176 (1998)
ARTICLE NO. CA981953

Dynamic Multiple Tracing with D_2 and C_2D_4 in Ethylene Hydroformylation over Mn–Rh/SiO_2

Mark A. Brundage[1] and Steven S. C. Chuang[2]

Department of Chemical Engineering, University of Akron, Akron, Ohio 44325-3906

Received July 21, 1997; revised October 24, 1997; accepted October 24, 1997

Combined FT-IR/mass spectrometry was used to study the dynamic behavior of hydrogen/deuterium adsorbates in response to D_2 and C_2D_4 pulses during ethylene hydroformylation on Mn–Rh/SiO_2 at 513 K and 0.1 MPa. Variation of exposure time of the catalyst to the D_2 and C_2D_4 pulses revealed that read-sorption did not play a significant role in the product responses; long exposure time allows more deuterium to enter the slower pathway of d_1- and d_2-propionaldehyde. The two-unequal-hump HD response from both the D_2 and C_2D_4 pulses indicates the presence of an isotope effect on hydrogen/deuterium adsorption. The rapid responses of the deuterated ethylene and ethane can be described by the Horiuti-Polanyi mechanism and indicate that their intermediates have small θ (surface coverage) and τ (residence time) which cannot be resolved by the time resolution of their transient responses. The d_1- and d_2-propionaldehyde products show a two-hump response, which can be explained by the different deuterium incorporation pathways into the propionaldehyde. The first hump is due to hydrogen/deuterium exchange on adsorbed acyl and acyl hydrogenation. The second hump is due to H/D exchange on the adsorbed alkyl species, which then undergoes CO insertion and acyl hydrogenation. The second hump decay is partly due to the reaction with Si–OD as indicated by the parallel decay of d_1- and d_2-propionaldehyde and Si–OD.

INTRODUCTION

Chemical reactions consist of a sequence of elementary steps in series and in parallel that convert reactants to products. The timescale of chemical reactions may range from a few femtoseconds (10^{-15} s) to geologic time (10^9 years or 10^{16} s) (1). Our ability to understand reaction mechanisms has primarily relied on advances in instrumentation which allows identification of intermediates and determination of reaction dynamics in the timescale of reaction relaxation. Various experimental techniques have been developed for studying the kinetics and dynamics of elementary steps of homogeneous reactions over a broad time range (1–4). The lack of interaction between elementary steps for homogeneous reactions allows isolation of each elementary step and intermediate in the overall reaction, and investigation of its kinetics and dynamics independently. The macroscopic kinetics of a homogeneous reaction can be obtained by integration of the kinetics of elementary steps (5).

Experimental techniques developed for studying the dynamics of homogeneous reactions are usually not applicable to the investigation of the dynamics of heterogeneous catalytic reactions which take place on catalyst surfaces (4, 6). The difficulty arises from interactions between adsorbates, influence of the reactivity of adsorbates by adsorption of reactants and products, and the transient nature of the intermediates (7, 8). These microscopic and dynamic characteristics are reflected by the strong dependence of kinetic parameters (pre-exponential factor and activation energy) of surface reactions on the adsorbate coverage and on the chemical environment of the catalyst surface in macroscopic kinetics and surface measurements. Therefore, the reactivity of adsorbates and the dynamics of surface reactions have to be studied under conditions where both reactants and products are present (6–12).

A time-resolved Fourier transform infrared (FT-IR)/mass spectrometer reactor system has been developed to study the reactivity of adsorbates and the dynamics of surface reactions under batch and steady-state flow conditions where both reactants and products are present (10, 13). The uniqueness of this technique is in the simultaneous measurement of the dynamics (i.e., transient response) of adsorbates and product concentration in a timescale which is in line with that of the evolution of adsorbates and products.

This paper reports the use of time-resolved FT-IR/mass spectrometer to study the dynamic behavior of adsorbed hydrogen/deuterium during ethylene hydroformylation on a Mn–Rh/SiO_2 catalyst. Hydroformylation is the reaction of an olefin with CO and H_2 to form aldehyde as the desirable product and paraffin as a by-product. The reaction has served as an excellent probe reaction for investigation of the CO insertion step in the Fischer-Tropsch synthesis (14, 15). The proposed heterogeneous ethylene hydroformylation mechanism is shown in Table 1 (13–16). The

[1] Present address: Delphi, Rochester, NY.
[2] To whom all correspondence should be addressed.

0021-9517/98 $25.00

TABLE 1

Ethylene Hydroformylation Mechanism

Step 1	$H_2 + 2^* \leftrightarrow 2^*H$	Hydrogen adsorption
Step 2	$CO + ^* \leftrightarrow ^*CO$	CO adsorption
Step 3	$C_2H_4 + ^* \leftrightarrow ^*C_2H_4$	Ethylene adsorption
Step 4	$^*C_2H_4 + ^*H \leftrightarrow ^*C_2H_5 + ^*$	Partial ethylene hydrogenation
Step 5	$^*C_2H_5 + ^*CO \leftrightarrow ^*C_2H_5CO + ^*$	CO insertion
Step 6	$^*C_2H_5CO + ^*H \leftrightarrow ^*C_2H_5CHO + ^*$	Acyl hydrogenation
Step 7	$^*C_2H_5 + ^*H \leftrightarrow C_2H_6 + 2^*$	Alkyl hydrogenation

* Indicates the surface site.

formation of two distinct hydrogenated products allows the use of hydroformylation as a model reaction to study the dynamics and the reactivity of adsorbed hydrogen in catalytic hydrogenation. The dynamics of the surface reaction involving adsorbed hydrogen was studied by pulse injection of D_2 into a steady-state H_2 flow while maintaining the CO and C_2H_4 flow rates at steady state and by pulse injection of C_2D_4 into a steady-state C_2H_4 flow while maintaining the CO and H_2 flow rates at steady state. Injection of D_2 allows tracing of the hydrogen/deuterium pathways and the dynamics of reactions involving hydrogen/deuterium during ethylene hydroformylation. Injection of C_2D_4 into the C_2H_4 stream allows tracing of the hydrogen/deuterium from adsorbed ethylene to determine their participation in the surface reactions. The length of time the catalyst was exposed to the D_2 and C_2D_4 pulses was varied by altering the total flow rate of the reactants to adjust the amount of deuterium entering hydrogen/deuterium pathways in order to probe the dynamics of various steps. Following pulse injection of deuterium, FT-IR is used to monitor the transient response of the deuterium-containing adsorbates on the catalyst surface; mass spectrometry is used to determine the response of the gaseous deuterium-containing products.

EXPERIMENTAL

Catalyst Preparation

A 4 wt% Mn–Rh/SiO_2 (Mn/Rh = 0.1) catalyst was prepared by a sequential incipient wetness method using an aqueous solution of $RhCl_3 \cdot 3H_2O$ (Alfa Products) and an aqueous solution of $Mn(NO_3)_2 \cdot 6H_2O$ onto a large pore SiO_2 support (Strem Chemicals, surface area of 350 m^2/g). After the impregnation sequence, the sample powder was dried in air at 298 K overnight and then was reduced in flowing H_2 at 673 K for 16 h (17).

Reaction Studies

Details of the IR reactor cell and the apparatus used in this study have been previously reported in detail (10, 15) and will be described briefly. Approximately 35 mg of catalyst powder was utilized in the study. Prior to each series of experiments the catalyst sample was reduced under H_2 flow at 673 K and 0.1 MPa for 2 h. The total flow rates of the reactants were varied from 60 to 240 cm^3/min at 513 K and 0.1 MPa. The IR reactor cell acts as a differential reactor to obtain the initial rates for the forward reaction.

Upon reaching the reaction steady-state for 15 min at the flow rate tested, the steady-state gaseous reactant and product concentrations were determined by an HP-5890A gas chromatograph (GC) equipped with a flame ionization detector (FID). Figure 1 illustrates the experimental procedure following the GC sample. A six-port valve was used to introduce a 10 cm^3 pulse of D_2 into the steady-state H_2 flow while maintaining CO, C_2H_4, and He flows at steady-state. During the pulse switch, the transient responses of the adsorbates on the catalyst surface were monitored by the IR spectrometer. Simultaneously, the transient responses of the gaseous effluent from the IR cell were recorded by a Balzers QMG 112 mass spectrometer (MS) that is interfaced to a computer that allows simultaneous measurement of eight *m/e* (i.e., amu) as a function of time. After completing the D_2 pulse, the six-port valve was used to introduce a 10 cm^3 pulse of C_2D_4 into the steady-state C_2H_4 flow while maintaining CO, H_2, and He flows at steady-state. Following steady-state and transient response studies, a bracketing reduction was performed to maintain the activity of the catalyst.

Product Analysis

Due to a one amu (*m/e*) resolution, the MS employed in this study is not able to separate these three pairs of deuterated products, d_2-ethylene and d_0-ethane (*m/e* = 30), d_3-ethylene and d_1-ethane (*m/e* = 31), and d_4- ethylene and d_2-ethane (*m/e* = 32) which have the same amu for their parent molecules. To determine the amount of deuterated ethylene and ethane produced, a GC-MS analysis was done for steady-state runs with $CO/D_2/C_2H_4$.

RESULTS

Table 2 reports the rate of product formation for the $CO/H_2/C_2H_4$ reaction for 4 wt% Mn–Rh/SiO_2 at 513 K and 0.1 MPa. The reaction produced C_2H_6 and C_2H_5CHO as major products with trace amounts of methane, propylene, 1-butene, and *n*-butane. The total flow rate of the reaction mixture was varied from 60 to 240 cm^3/min. The difference in pressure drops for CO, H_2, and C_2H_4 lines before the mixing point caused an alteration in the flow rates, thus leading to a slight change in the partial pressures of the reactants, as indicated by the $CO/H_2/C_2H_4$/He ratio in Table 2. This change in reactant partial pressure did not cause a significant change in propionaldehyde selectivity.

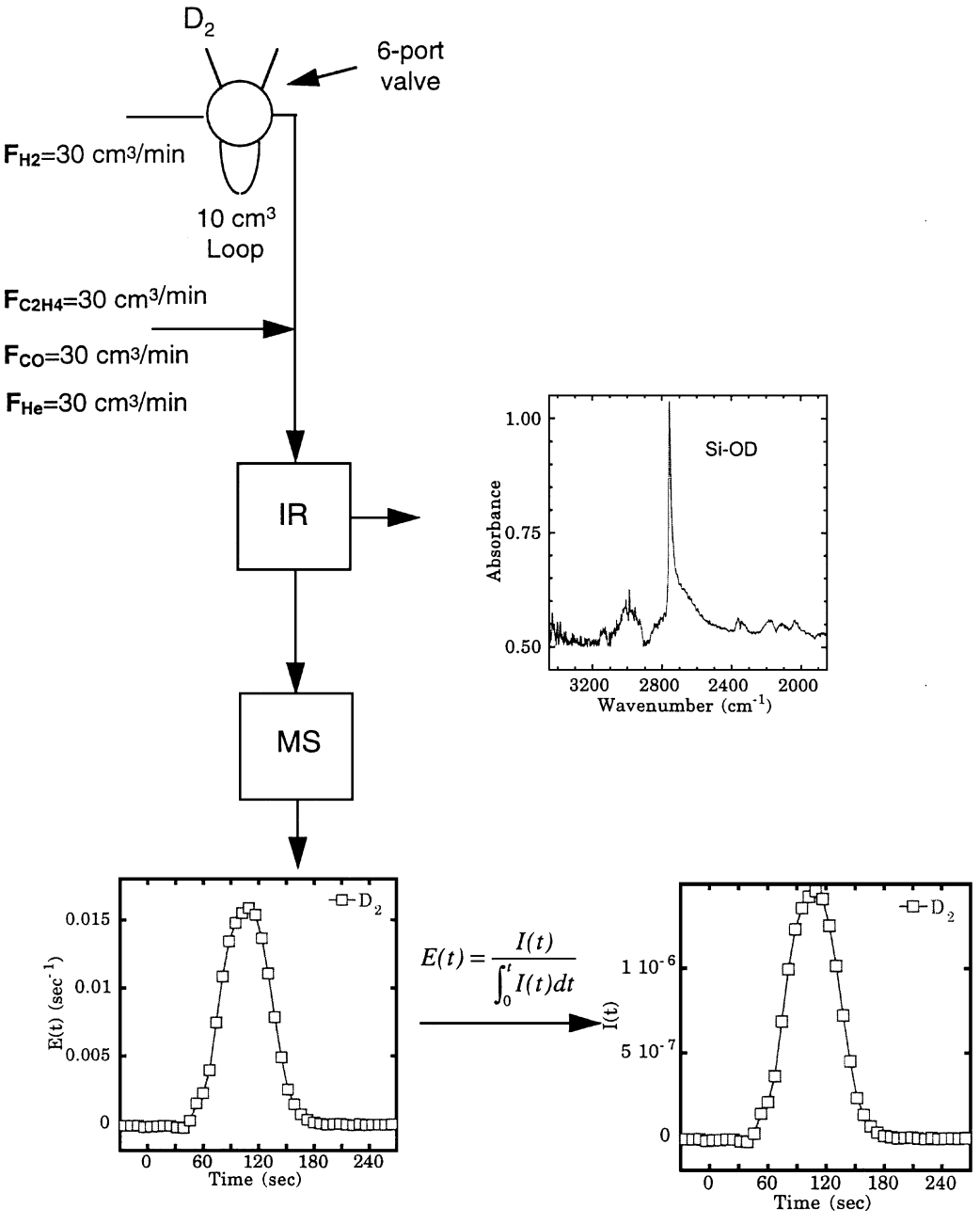

FIG. 1. Experimental setup.

Transient Response to a D_2 Pulse

Figure 2 shows the normalized deuterated products and IR response for Si–OD to a 10 cm^3/min D_2 pulse into the steady stream of H_2 at a total flow rate of 60 cm^3/min. The pulse response is normalized using the equation

$$E(t) = \frac{I(t)}{\int_0^\infty I(t)\,dt}, \qquad [1]$$

where $I(t)$ is the MS intensity, which can be related to the concentration by a calibration factor, during the transient response (10, 15, 18). For instance, $E(t)$ for H_2 is normalized from the intensity of H_2. The normalized responses allow accurate determination of the lead-lag relationship for the reactants and products. Contained in the hydrogen stream is 2% Ar, which is inert and does not interact with the catalyst surface. The inertness of Ar allows it to be utilized as a tracer to obtain the flow pattern of the reactor and to determine the contribution of the reactant flow to the reactant and product responses. Figure 2a shows that the H_2, D_2, and HD responses lagged behind the Ar response. The delay of the Ar response is due to the transportation time in

TABLE 2

The Rate and Selectivity for Product Formation during $CO/H_2/C_2H_4$ Reaction

	Turnover frequency (min^{-1})		
Total flow rate	60 cm^3/min	120 cm^3/min	240 cm^3/min
$CO/H_2/C_2H_4$/He	0.9/1.1/0.9/1.1	1/1/1/1	1.1/0.9/1/1
Methane	0.015	0.026	0.032
Ethane	2.9	3.9	2.9
Propylene	0.028	0.057	0.028
1-Butene	0.007	0.015	0.006
n-Butane	0.010	0.021	0.005
Propionaldehyde	0.22	0.27	0.28
Selectivity[a]	0.075	0.069	0.098

Note. Adsorption stoichiometry: $H/metal_{atom} = 1$ (19, 35). Hydrogen chemisorption: 114 μmol *H/g_{cat}. Rh crystallite size: 14 Å.

[a] Rate of formation of propionaldehyde divided by rate of formation of ethane.

the tubing. The H_2 and D_2 responses lag behind the Ar response as a result of adsorption, reaction, and desorption of H_2 and D_2 on the catalyst surface. The H_2 and D_2 responses were nearly symmetrical, indicating the total concentration of H_2 and D_2 was maintained at steady state during the pulse. The average residence time for H_2, τ_{H_2}, can be obtained by $\tau_{H_2} = \int_0^t t^* E_{H_2}(t)\, dt$ (10, 15). The residence time of adsorbed hydrogen (*H) on the catalyst surface is determined by $\tau_{*H} = \tau_{H_2} - \tau_{Ar}$ (10, 15), where τ_{*H} is 15.0 s and τ_{*D} is 21.9 s, indicating the presence of an isotope effect on H_2/D_2 adsorption. The HD response showed a two-hump response. The first hump slightly led the D_2 response while the second hump lagged behind the D_2 response. The minimum between the two humps corresponds to the minimum point on the H_2 response; the maximum point on each hump occurs at the point where the gaseous hydrogen and deuterium concentrations are equal during the pulse transient.

Figures 2b and 2c show selected deuterated ethylene, ethane, and propionaldehyde responses from the D_2 pulse, where d_i represents the i number of deuterium atoms in the product species. The d_1-ethylene (C_2H_3D) and d_1-ethane (C_2H_5D) responses closely matched with that of the D_2 response, as did the other deuterated ethylene and ethane responses. Assuming that the formation of deuterated ethylene and ethane follows a first-order response, the rate of formation (i.e., TOF) can be expressed as $TOF = k\theta = \theta/\tau$ (10–12, 15), where k is the first-order rate constant, θ is the surface coverage, and τ is the residence time for intermediates leading to the product. The evolution rate of deuterated ethylene and ethane is significantly greater than the convection and diffusion rates of the reactant mixture, thus blurring the reactant and C_2 hydrocarbon product responses. The overlapping of the reactant and product response curves indicates that the ethylene adsorption/desorption step (step 3 in Table 1), the partial hydrogenation step (step 4), and the hydrogenation of the adsorbed alkyl species step (step 7) all have a very high k and low θ for their intermediates. θ for the ethyl intermediate has been estimated to be 0.04 for ethylene hydrogenation

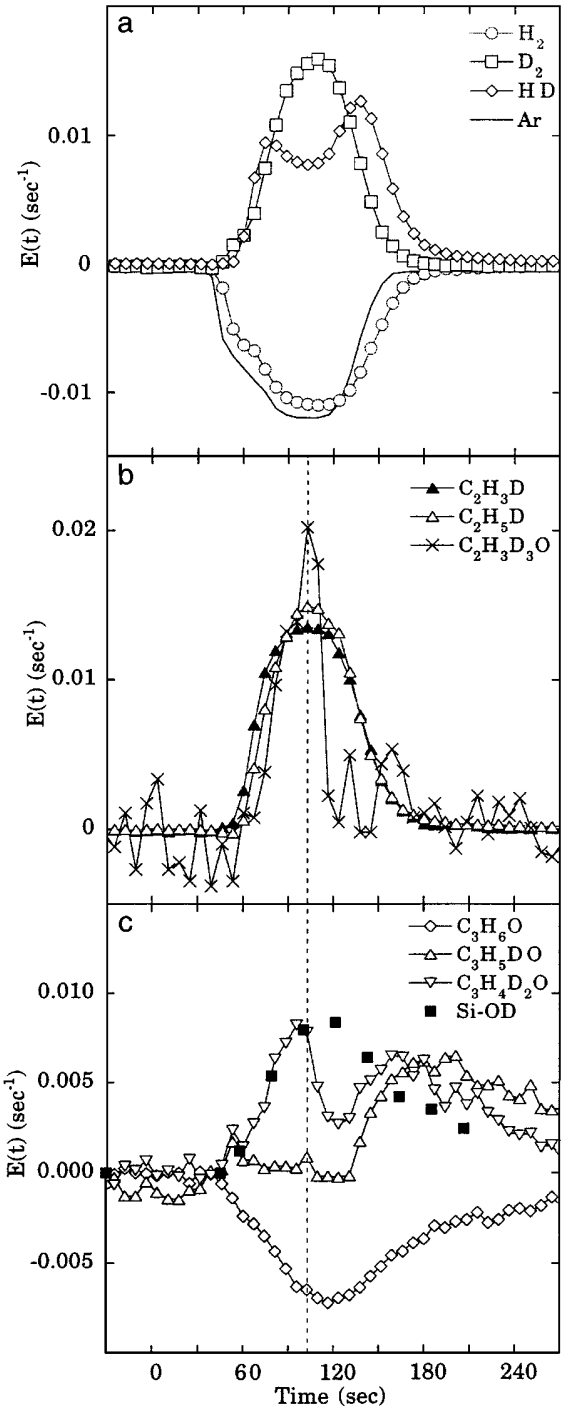

FIG. 2. Normalized transient responses to a D_2 pulse into H_2. (a) H_2, D_2, and HD, (b) C_2H_3D, C_2H_5D, and $C_3H_3D_3O$; deuterated ethylene, (c) d_0-propionaldehyde, d_1-propionaldehyde, d_2-propionaldehyde Si–OH, and Si–OD. All at 513 K and 0.1 MPa; total flow rate = 60 cm^3/min; $t = -40$ is the time at which the pulse injection of D_2 was made.

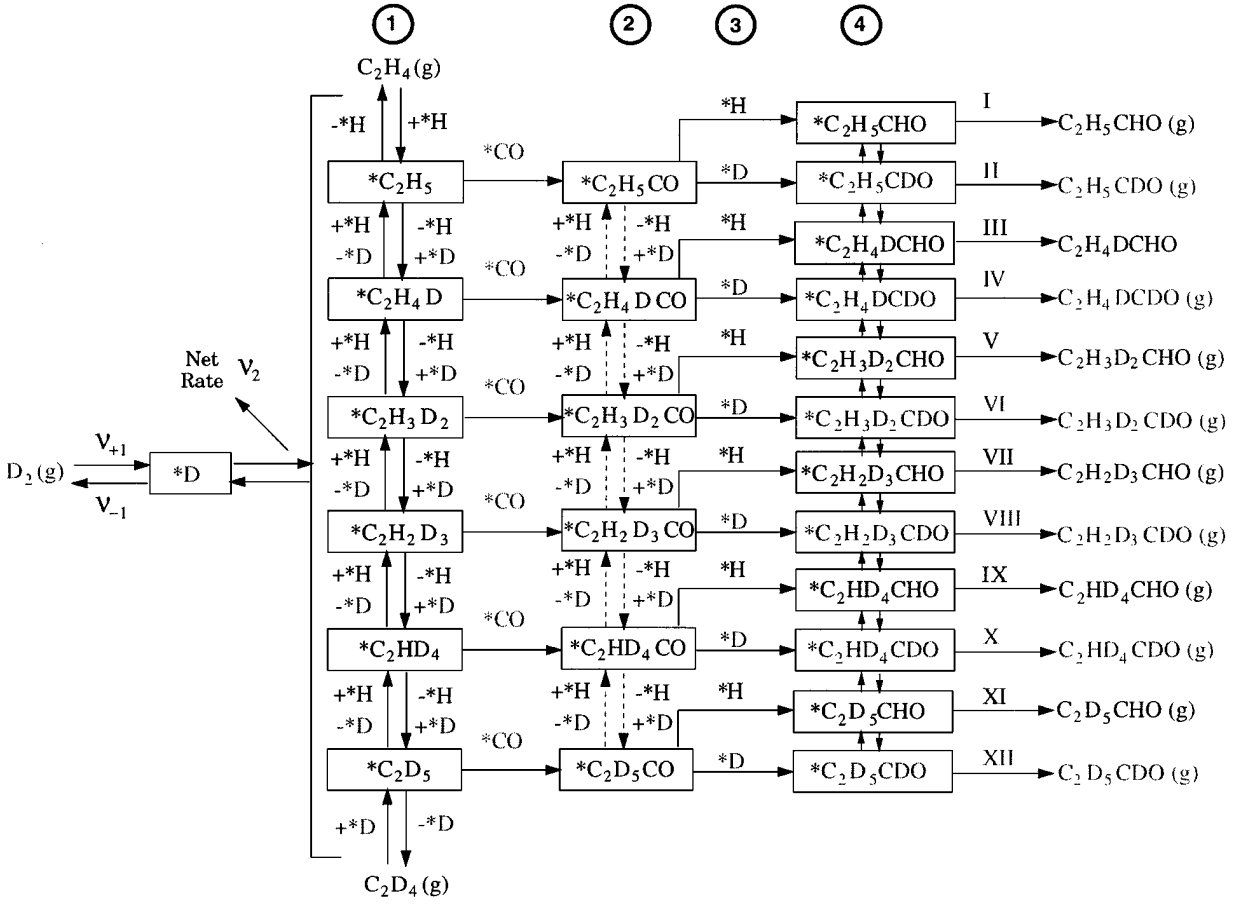

FIG. 3. Proposed mechanism for deuterium product incorporation. ① Partial ethylene hydrogenation/dehydrogenation, ② hydrogenation/ deuterium exchange on adsorbed acyl, ③ deuteration of the adsorbed acyl species, and ④ hydrogen/deuterium exchange on adsorbed propionaldehyde.

on Pt at 295 K (19). Using this value of θ as a conservative estimate for our experimental conditions and the TOF for ethane formation in Table 2, τ is calculated to be less than 1 s, which is below the resolution of our MS.

The d_0-propionaldehyde (C_3H_6O), d_1-propionaldehyde (C_3H_5DO), and d_2-propionaldehyde ($C_3H_4D_2O$) responses shown in Fig. 2c have distinctly different responses as compared to the D_2 response. The formation of the various deuterated propionaldehyde products can be best illustrated by the reaction pathway shown in Fig. 3. Although the pathway shown in Table 1 and Fig. 3 did not distinguish between the sites for ethane and propionaldehyde formation, selective poisoning and alkali promotion studies have shown that the active sites for ethane and propionaldehyde formation are different (13, 14).

Figure 3 shows the proposed compartment model and reaction pathways for the formation of hydrogen- and deuterium-containing propionaldehyde from pulse injection of D_2 and C_2D_4. The adsorbates distributed on the catalyst surface are lumped into boxes (pools). Within each box, the species are considered well-mixed and the isotope-labeled species transfers from one pool to another according to the proposed pathway. In this mechanism, deuterium may enter the propionaldehyde product in four ways: ① partial ethylene hydrogenation/dehydrogenation, ② hydrogenation/deuterium exchange on adsorbed acyl, ③ deuteration of the adsorbed acyl species, and ④ hydrogen/deuterium exchange on adsorbed propionaldehyde. The first, second, and fourth pathways allow deuterium to enter the alkyl group of the propionaldehyde; the third and fourth pathways allow deuterium to enter the formal group (−CHO). The different isomers of d_i-propionaldehyde can not be resolved by our MS, complicating analysis of the pathway for formation of these products.

The d_1-propionaldehyde response showed a small initial response but then quickly decreased on the $E(t)$ scale until 135 s where it again increased, showing a two-hump response. The two-hump response may be due to the different deuterium positions of the different isomers, C_2H_4DCHO and C_2H_5CDO, from different pathways. Similar to d_1-propionaldehyde, the d_2-propionaldehyde response also showed a two-hump response, though its first hump was much more significant than the d_1-propionaldehyde first hump. The higher deuterated propionaldehyde responses,

TABLE 3

Deuterium Distribution within Deuterated Propionaldehyde Products

	60 cm^3/min		120 cm^3/min		240 cm^3/min	
	First hump	Second hump	First hump	Second hump	First hump	Second hump
			D_2			
d_1-propionaldehyde	1.8%	52%	13%	33%	27%	9.9%
d_2-propionaldehyde	6.2%	26%	14%	16%	23%	3.9%
d_3-propionaldehyde	5.9%	—	14%	—	13%	—
d_4-propionaldehyde	4.7%	—	5.7%	—	13%	—
d_5-propionaldehyde	2.8%	—	4.9%	—	10%	—
			C_2D_4			
d_1-propionaldehyde	3.7%	18%	8.0%	4.2%	26%	3.9%
d_2-propionaldehyde	10%	32%	30%	5.7%	29%	4.2%
d_3-propionaldehyde	17%	—	27%	—	21%	—
d_4-propionaldehyde	12%	—	17%	—	10%	—
d_5-propionaldehyde	6.9%	—	8.8%	—	5.9%	—

represented by d_3-propionaldehyde ($C_3H_3D_3O$) in Fig. 2b, did not show this two-hump response and had single-hump pulse responses that closely followed the D_2 response. Drawing a dashed line through the peak of d_3-propionaldehyde to the d_2-propionaldehyde response shows that the d_3-propionaldehyde response coincides with the first hump of the d_2-propionaldehyde response.

Determination of the deuterated propionaldehyde distribution within each propionaldehyde hump will give insight into the deuterium incorporation mechanism. Because of the absence of calibration standards, accurate quantification of each d_i-ethylene, d_i-ethane, and d_i-propionaldehyde could not be completed. However, assuming that the area of each species under the $I(t)$ the response curve is proportional to the amount of products produced, the relative amount of each d_i-propionaldehyde can be calculated and is shown in Table 3. The total d_i-propionaldehyde distribution between the first and second hump responses sums to 100%. The relative amount of deuterated propionaldehyde is primarily contained within the second hump. The first hump contains d_1- through d_5-propionaldehyde, with d_2- and d_3-propionaldehyde being the major products while the second hump only contains the d_1- and d_2-propionaldehyde products.

Figure 4 shows the transient IR response to the D_2 pulse. Gas phase CO at 2150 and 2082 cm^{-1} and adsorbed linear CO at 2020 cm^{-1} were not altered by the D_2 pulse. The main feature of IR spectra during pulsing D_2 is the growth and decay of the Si–OD band at 2755 cm^{-1} (17, 20, 21). The growth of the Si–OD band indicates that deuterium can migrate or spill over from the metal surface to the silica support. The decay of the Si–OD indicates that reverse spillover of deuterium from the silica support to the metal surface also occurs. A vague change in the Si–OH stretch at 3744 cm^{-1} was also observed. The area under the Si–OD IR spectra, which is equivalent to concentration of OD, was determined by

$$A_{OD} = \int_{2650}^{2800} A(\nu)\, d\nu, \qquad [2]$$

where $A(\nu)$ is the absorbance and ν is the wavenumber in cm^{-1}. A normalized $E(t)$ response for the Si–OD area response was determined and is plotted in Fig. 2c for comparison with d_0-, d_1-, and d_2-propionaldehyde responses. The lag time between D_2 and Si–OD reflects the time required for spillover of adsorbed deuterium from the metal surface to the silica support. Surprisingly, the decay responses of Si–OD lagged significantly behind that of the D_2 response. The slow decay of Si–OD as compared with its rapid rise indicates that the rate of deuterium spillover

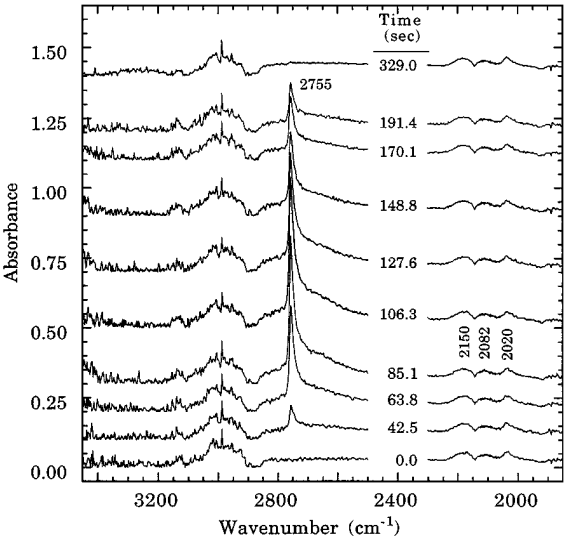

FIG. 4. *In situ* IR transient responses to a D_2 pulse into H_2 at 513 K, 0.1 MPa and total flow rate = 60 cm^3/min.

from the metal to the silica surface is higher than the rate of the reverse deuterium spillover from the silica surface back to the metal. The difference in the rate of forward and reverse spillover could be related to the different concentration of adsorbed deuterium on Rh and Si–OD on the SiO_2 surface.

Direct D_2 adsorption studies on SiO_2 did reveal a slow formation of the Si–OD peak at 2755 cm^{-1}; the maximum absorbance on SiO_2 was 20 times less than that observed on Mn–Rh catalyst during the D_2 pulse. The growth of the Si–OD peak on SiO_2 was also much slower than that on Mn–Rh/SiO_2, as shown by the larger τ for SiO_2 (217 s) than for Mn–Rh/SiO_2 (115 s). This result indicates that the direct formation of Si–OD from D_2 adsorption on SiO_2 and other adsorption processes do not make a significant contribution to the Si–OD response on Mn–Rh/SiO_2 during the transient experiments.

Transient Response to a C_2D_4 Pulse

The normalized deuterated product responses to a 10 cm^3 pulse injection of C_2D_4 into the steady-state flow of C_2H_4 are shown in Fig. 5. Figure 5a shows that the D_2 response had a sharper response than the C_2D_4 response, indicating that deuterium was rapidly transferred from the C_2D_4 to the catalyst surface for desorption. The decrease in C_2H_4 concentration caused a decrease in gaseous hydrogen concentration further confirming that ethylene is a source of hydrogen. The HD response also showed a two-hump response, resembling that from the D_2 pulse. Figures 5b and 5c show selected deuterated ethylene, ethane, and propionaldehyde responses. Similar to the D_2 pulse results, the d_1-ethylene (C_2H_3D) and d_1-ethane (C_2H_5D) responses closely matched that of C_2D_4, supporting the earlier conclusions of rapid ethylene adsorption/desorption and partial ethylene hydrogenation with small τ and θ.

Figure 5c shows the d_0-propionaldehyde, d_1-propionaldehyde, and d_2-propionaldehyde responses. Both the d_1-propionaldehyde and the d_2-propionaldehyde responses also revealed the two-hump response, although it was less distinct than during the D_2 pulse. The higher deuterated propionaldehyde responses represented by d_3-propionaldehyde in Fig. 5b showed single-hump responses, similar to the C_2D_4 response. Analysis of the relative amounts of deuterated propionaldehyde product responses are shown in Table 3. Observations were made for the C_2D_4 pulse similar to those for the D_2 pulse results, with d_1- through d_5-propionaldehyde in the first hump going through a maximum and only d_1- and d_2-propionaldehyde in the second hump.

The IR response to the C_2D_4 pulse into C_2H_4 was similar to that of the D_2 pulse, with the major variation in the IR spectra being the Si–OD peak at 2755 cm^{-1} that developed and disappeared. Comparing the relative IR area of the Si–OD response of the D_2 pulse to that of the C_2D_4 pulse revealed that about 10 times less deuterium spillover occurred during the C_2D_4 pulse than during the D_2 pulse. The normalized IR intensity response of the Si–OD peak for the C_2D_4 pulse switch is plotted in Fig. 5c.

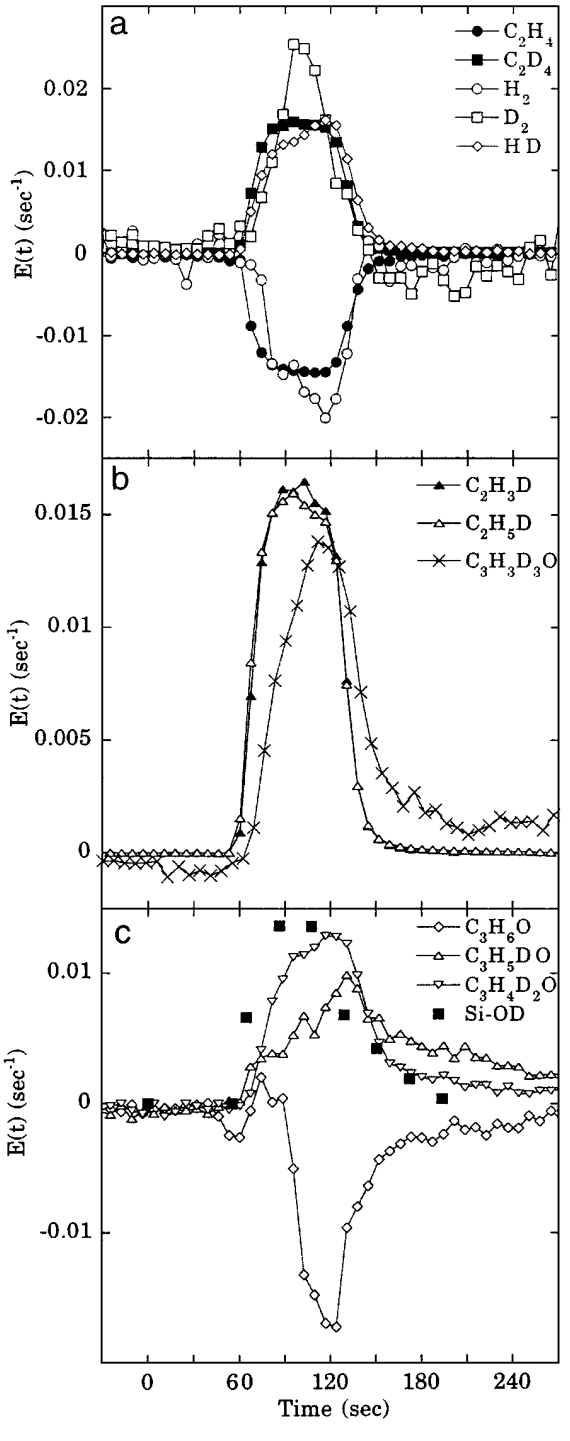

FIG. 5. Normalized transient responses to a C_2D_4 pulse into C_2H_4. (a) H_2, D_2, and HD, (b) C_2H_3D, C_2H_5D, and $C_3H_3D_3O$ deuterated ethylene, (c) d_0-propionaldehyde, d_1-propionaldehyde, d_2-propionaldehyde, and Si–OD. All at 513 K and 0.1 MPa. Total flow rate = 60 cm^3/min.

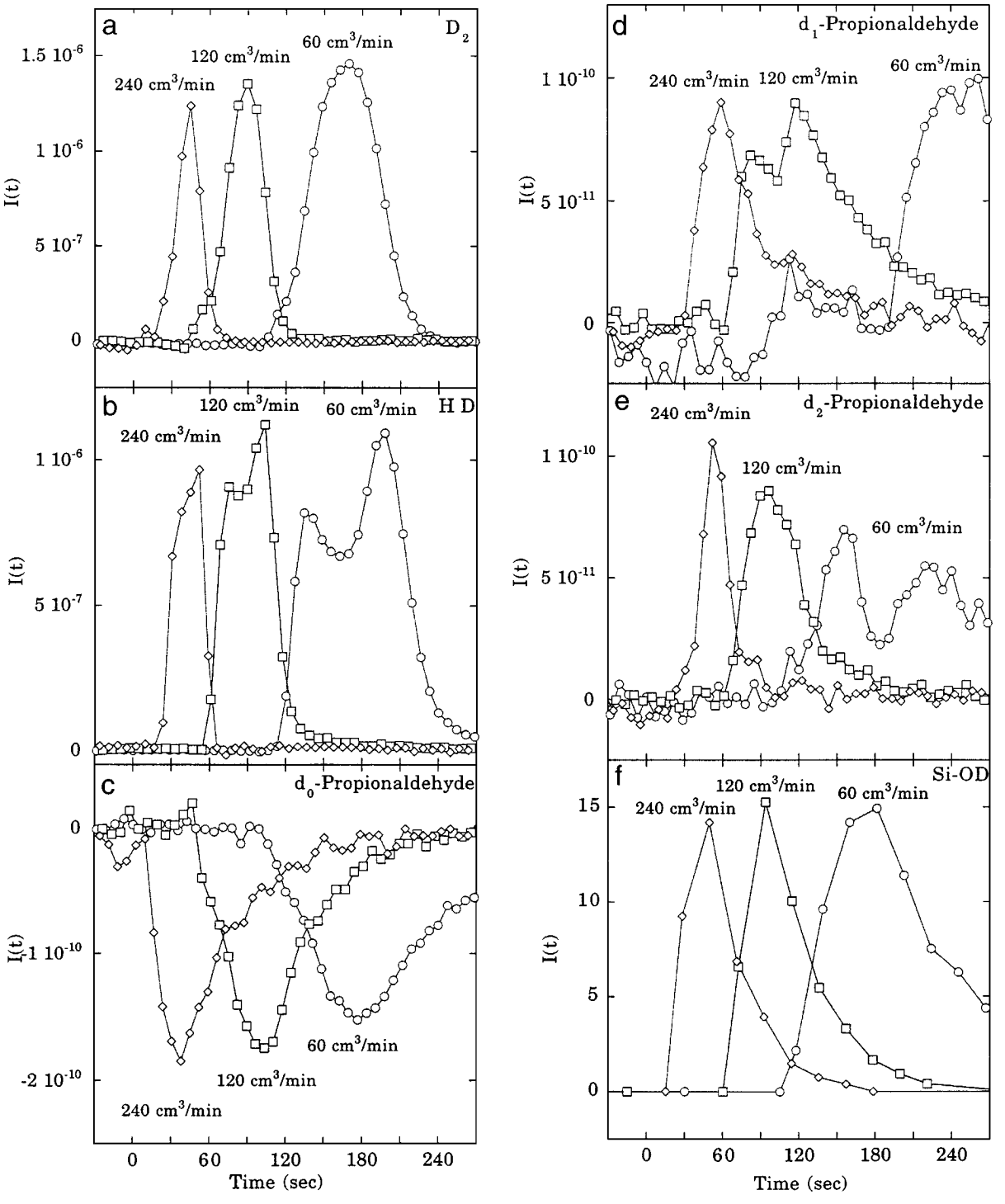

FIG. 6. Responses to a D_2 pulse into H_2 as a function of flow rate. (a) D_2, (b) HD, (c) d_0-propionaldehyde, (d) d_1-propionaldehyde, (e) d_2-propionaldehyde, (f) Si–OD. $t = 0$ is the time at which the pulse injection of D_2 was made.

Effect of Tracer Residence Time

The objective of these experiments is to determine the effect of flow rate on the transient responses of the deuterated products and the readsorption effect on the products. The isotopic pulse into the different flow rates caused different product flow pattern responses. Figure 6 shows the effect of increasing the total flow rate from 60 to 240 cm^3/min on selected deuterated products on the D_2 pulse into H_2. Figure 6a shows that the 60 cm^3/min D_2 response came out

the slowest and had the broadest response. Increasing the flow rate caused a faster and sharper response as compared to the 60 cm^3/min response. $I(t)$, which is equivalent to the concentration of the species, cannot be used for comparison of the concentration of the species monitored in different flow rate runs due to slightly different total pressures at the MS sampling point for these runs.

Figure 6b shows the effect of increasing the flow rate on the two-hump HD response. Increasing the flow rate caused the HD two-hump response to apparently merge into a single hump. However, the similarity in contours of the different flow rate HD responses suggests that the two-hump response still exists, although it has become blurred due to the convection and diffusion of the gaseous flows. Therefore, the change in flow rate did not alter the hydrogen and deuterium adsorption and reaction characteristics of the catalyst.

Figure 6c shows that the d_0-propionaldehyde responses all are single-hump responses. Figure 6d shows that increasing the flow rate from 60 to 120 cm^3/min caused the two-hump d_1-propionaldehyde response to overlap; increasing the flow rate to 240 cm^3/min caused an increase in the first hump response and a decrease in the second hump response. Figure 6e shows that increasing the flow rate also caused a similar shift for the d_2-propionaldehyde response. Figure 6f shows that increasing the flow rate did not affect the relative intensity of Si–OD. The C_2D_4 pulse responses showed similar flow effects on the product responses and are not shown here.

Table 3 shows that increasing the flow rate caused the deuterated propionaldehyde distribution to shift from the second hump to the first hump. Increasing the flow rate also caused a shift of the deuterium substitution to the lower deuterated propionaldehyde for the first hump response while increasing the flow rate had minimal effect on the relative deuterated propionaldehyde distribution in the second hump, with a d_1-propionaldehyde/d_2-propionaldehyde ratio of about 2.

To minimize the effect of flow rate on the contours of the responses, a dimensionless time, Θ, that accounts for the effect of different flow rates is used for normalizing the time scale. Θ, which is defined by $\Theta = (\nu_0/V)^*t$, where ν_0 is the total volumetric flow rate, and V is the system volume, allows for fair comparison of the transient responses at the various flow rates (22). Figure 7 shows the D_2 $I(\Theta)$ response versus Θ. The similar responses for D_2 suggest that the change in flow rate did not affect the D_2 adsorption and surface reaction processes of the catalyst. The same can be stated for the deuterated ethylene and ethane responses because of the similarity of their responses to the D_2 responses at the different flow rates.

Figure 7b shows the $I(\Theta)$ versus Θ of the d_1-propionaldehyde response to the D_2 pulse. The first hump response is altered by the change in flow rate as shown by

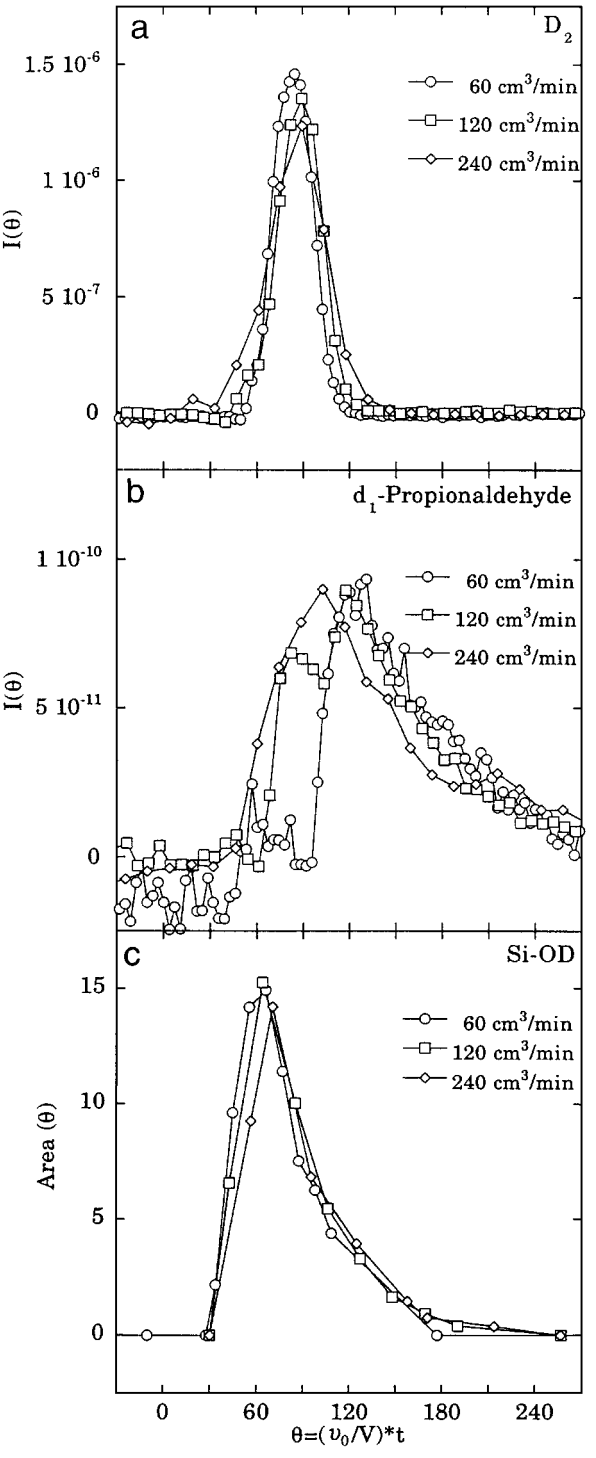

FIG. 7. Normalized time comparison of Fig. 6. (a) D_2, (b) d_1-propionaldehyde, (c) Si–OD.

the increase in the relative amount of product formation in the first hump as compared to the second hump. The absence of significant variation in the decay portion of the response curves for the d_0-propionaldehyde and

d_1-propionaldehyde responses suggests readsorption does not play a significant role in the deuterated propionaldehyde responses (17). Figure 7c shows the Si–OD response versus Θ. The Si–OD responses are all similar, indicating the spillover ability of the catalyst also is not affected by the change in flow rate.

DISCUSSION

Dynamics of $^*H$ from H_2 and C_2H_4

The formation of HD during the D_2 and C_2D_4 pulses may proceed via the elementary steps

$$H_2 + 2^* \leftrightarrow 2^*H$$
$$D_2 + 2^* \leftrightarrow 2^*D$$
$$^*H + {}^*D \rightarrow HD + 2^*.$$

The formation of the two-hump HD response is a result of the increase and decrease in hydrogen and deuterium concentration during the D_2 pulse into H_2. The rate of these steps is higher than that of convection and diffusion of the species in the flow. The maximum of the first and second hump occurs when $\theta_{*H} = \theta_{*D}$, which corresponds to about when $P_{H_2} = P_{D_2}$. The first hump occurs when θ_{*H} is decreasing and θ_{*D} is increasing and results from $^*H + D_2 \rightarrow HD + {}^*D$, which is written in terms of the overall reaction, due to the fact that only $^*H$ is available on the catalyst for reaction with $^*D$ from the dissociative adsorption of the pulsed D_2. The second hump occurs when θ_{*H} is increasing and θ_{*D} is decreasing and results from $^*D + H_2 \rightarrow HD + {}^*D$. The larger response of the second hump indicates the reaction of H_2 with $^*D$ is faster than the reaction of D_2 with $^*H$, suggesting the presence of an isotope effect on hydrogen/deuterium adsorption. The isotope effect originates from the large mass and bonding energy differences between the molecular species and its isotopic counterpart (23, 24).

To confirm that changing the total flow rate did not change the rate of adsorption and desorption, modeling of the deuterium adsorption step was undertaken. Figure 8 shows the mole balances considering only the D_2 and the $^*D$ pools from Fig. 3 (17) and illustrates the modeling procedure. Since D_2 traveled with Ar at the same flow rate and pattern, E_{Ar} should be considered as the input E_{D_2}. Step 1 involves the fitting of the 120 cm^3/min flow rate D_2 response to the model response curve to generate the following fitted parameters: rate of adsorption, ν_{+1d}; rate of desorption, ν_{-1d}; and the coverage of adsorbed deuterium on the catalyst surface, θ_{*D}, presented in Fig. 8. Step 2 shows that using these fitted parameters and changing the input E_{Ar} response and the $Q^{in}_{D_2}$ to the appropriate value, the output E_{D_2} responses for the other flow rates can be generated. If the flow rate has no effect on the rate of adsorption, desorption, and surface coverage, then the generated E_{D_2} responses for the 60 and 240 cm^3/min flow rates using the fitted parameters for ν_{+1d}, ν_{-1d}, and θ_{*D} from the 120 cm^3/min flow rate should match the experimental data for the 60 and 240 cm^3/min flow rates.

Figure 9 shows that the model results match well with the experimental data points for all the flow rates, indicating that (i) changing the total flow rate did not alter the hydrogen adsorption, desorption, and total hydrogen coverage of the catalyst, and (ii) readsorption did not occur to a significant extent. Comparing the H_2 and D_2 response model results, an isotope effect of 1.2 was found for hydrogen/deuterium adsorption for the ratio of θ_{*H} to θ_{*D}.

Determining the deuterium distribution in ethylene and ethane provides information for determining the relative rate of each step involving deuterium. Because of the overlap of some of the *m/e* ratios for deuterated ethylene and ethane as described in the experimental section, GC-MS analysis was used to obtain steady-state deuterated ethylene and ethane product distributions. The results listed in Table 4 revealed the production of both deuterated ethylene and ethane products, which can be described by steps 1, 3, 4, and 7 from Table 1. These reaction steps are consistent with those in the Horiuti–Polanyi mechanism for ethylene hydrogenation (19, 25–28):

$$\begin{array}{ccccc} & & {}^*C_2H_3 + {}^*H & & \\ & & \uparrow & & \\ C_2H_4 & \overset{3}{\rightleftharpoons} & \left.\begin{matrix} {}^*C_2H_4^* \\ {}^*C_2H_4 \end{matrix}\right\} & \overset{4}{\rightleftharpoons} {}^*C_2H_5 & \left.\begin{matrix} \\ \\ \end{matrix}\right\} \overset{7}{\rightarrow} C_2H_6. \\ & H_2 \overset{1}{\rightleftharpoons} & \left\{\begin{matrix} {}^*H \\ {}^*H \end{matrix}\right. & \dashrightarrow & \end{array}$$

All the postulated intermediates shown in the above pathway for the Horiuti–Polanyi mechanism have been recently observed by sum frequency generation (SFG) spectroscopy under reaction conditions (19). Both π-bonded ethylene ($^*C_2H_4$) and di-σ bonded ethylene ($^*C_2H_4^*$) have been shown to be precursors for ethylene hydrogenation. The π-bonded ethylene is much more active for hydrogenation than the di-σ bonded ethylene at 295 K (19). The di-σ bonded ethylene is also a precursor for dehydrogenation to the ethylidyne species ($^*C_2H_3$). This species can also be hydrogenated, but at a slower rate than the di-σ bonded ethylene at 295 K (19). Although it is anticipated that all the steps are rapid at our experimental temperature, the absence of statistical distribution of deuterium in the products in Table 4 indicates product formation is kinetically controlled. The relative amounts of deuterated ethylene and ethane therefore can be utilized to distinguish the relative rates of steps 3, 4, and 7.

Table 4 shows that more deuterated ethylene is produced as compared to deuterated ethane, indicating that steps 3 and 4 are faster than step 7. The increased production of lower deuterated ethylene also suggests the backward rate

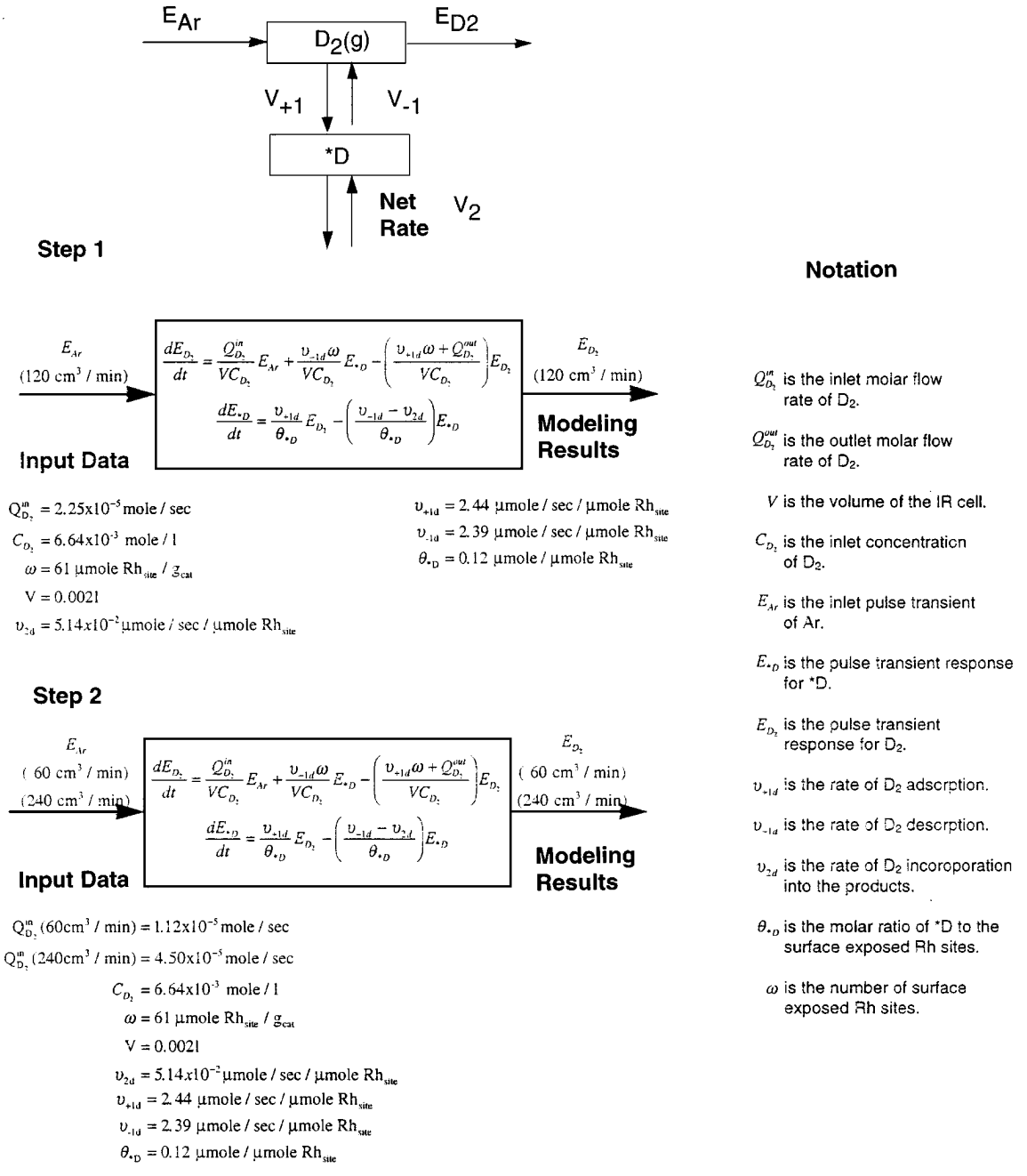

FIG. 8. Compartment model.

of steps 3 and 4 is faster than the forward rate of step 7. Studies at different temperatures on Rh revealed that increasing the temperature caused a larger increase in intensity for the deuterated ethane than for the deuterated ethylene (29), indicating ethane formation requires a higher activation energy. It is interesting to note that Horiuti and Polanyi provided a decisive mechanism which accurately describes our deuterated product distribution (including d_0-ethane), as well as others (19, 30–32), without experimental observation of adsorbates.

Deuterated Propionaldehyde Responses

The variation of the d_1- and d_2-propionaldehyde responses with flow rate during the D_2 and C_2D_4 pulses reveals the difference in the relative rate constants and the reaction pathways for their formation. The increase in flow rate decreased the exposure time of the catalyst to the D_2 pulse, shifting the d_1- and d_2-propionaldehyde responses from the second hump to the first hump. The shift in deuterium distribution indicates deuterium incorporation

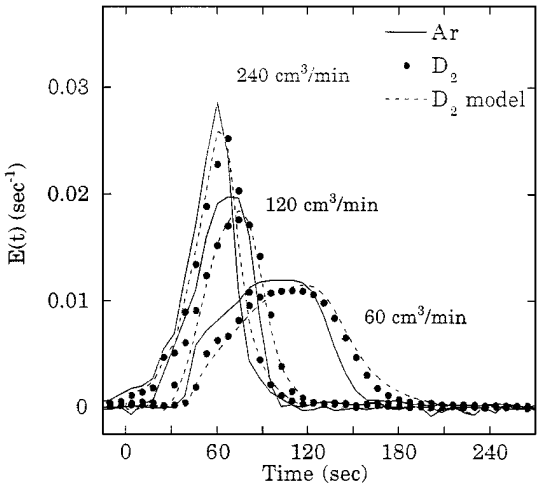

FIG. 9. Comparison of D_2 model and experimental responses.

into the first hump is faster than deuterium incorporation into the second hump. Our recent studies show that the τ for the first hump is approximately the same as the τ for the d_1- and d_2-propionaldehyde responses from the pulse reaction of D_2 with $CO/H_2/C_2H_4/C_2H_5CHO$. The first hump d_1-propionaldehyde may result from exchange between adsorbed deuterium with the adsorbed acyl species or the adsorbed enol species. The formation of adsorbed enol intermediates from the adsorption of C_2H_5CHO would allow deuterium to enter the α position via keto-enol tautomerism.

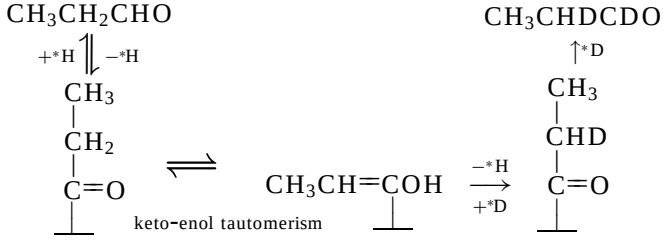

Both enol intermediates and keto-enol tautomerism have been suggested as the primary intermediates and pathway for higher alcohol formation from syngas (33, 34). The tautomerism is known to be a rapid process which would give a low τ for the d_i-propionaldehyde from the pulse reaction of D_2 with $CO/H_2/C_2H_4/C_2H_5CHO$ (29). The low τ for the first hump d_1- and d_2-propionaldehyde allows adsorbed deuterium to enter their alkyl group with a short deuterium exposure time. The shorter deuterium exposure time shifted the deuterium distribution to the first hump as shown in Table 3.

The second hump propionaldehyde response may result from the insertion of CO into the adsorbed $C_2H_xD_{5-x}$ and the subsequent deuteration of the adsorbed acyl species. The $C_2H_xD_{5-x}$ in d_i-propionaldehyde may share the same alkyl precursor as that for d_i-ethane. The τ for the second hump response has also recently been found in the range of τ for the formation of $C_2H_5{}^{13}CHO$ from the ^{13}CO pulse study, further confirming that the second hump is a result of CO insertion into the adsorbed alkyl species which has undergone limited hydrogen/deuterium exchange.

Mn promoter has been shown to stabilize the acyl intermediate species on Rh catalyst (35), which increases the likelihood of hydrogen/deuterium exchange to occur on the adsorbed acyl/enol species causing the first hump propionaldehyde response. Comparison of previous results on d_1-propionaldehyde and d_2-propionaldehyde responses on Rh/SiO_2 and $Mn–Rh/SiO_2$ shows that Mn promoter increases the deuterium distribution in the first hump. These results further support the proposition that the first hump is due to hydrogen/deuterium exchange on the adsorbed acyl/enol (shown as dashed arrows in Fig. 3), followed by hydrogenation/ deuteration of the adsorbed acyl species.

In Situ Infrared Observation of Si–OD

The *in situ* infrared technique employed in this study was not able to provide unambiguous information on hydrogenation/deuteration of hydrocarbon intermediates due to low extinction coefficients of C–H and C–D stretching and overlapping of these bands. The most valuable information obtained from the *in situ* IR studies is the spillover of adsorbed deuterium from the Rh surface to the Si–OD site and the involvement of deuterium from Si–OD for deuteration of the adsorbed acyl. The latter is supported by the experimental results: (i) parallel decay of the d_1-propionaldehyde and d_2-propionaldehyde second hump responses with that of the Si–OD response, as seen in Figs. 2c and 5c, and (ii) pulsing C_2D_4 resulted in less Si–OD formed as compared to the D_2 pulse, resulting in less d_1- and d_2-propionaldehyde formed, as seen in Table 3. The slow Si–OD response as compared to the D_2 response can be attributed to the surface diffusion of the deuterium on the silica surface (21).

TABLE 4

Deuterium Distribution in Ethylene and Ethane Products from Steady-State Ethylene Hydroformylation at 120 cm³/min

	$CO/D_2/C_2H_4$		$CO/H_2/C_2D_4$	
d_i	Ethylene	Ethane	Ethylene	Ethane
d_0	—	2.6%	—	6.1%
d_1	73%	1.2%	12%	6.4%
d_2	17%	0.94%	40%	15%
d_3	3.8%	0.39%	18%	1.7%
d_4	0.79%	—	—	0.25%

CONCLUSIONS

Transient responses of deuterated products to the D_2 and C_2D_4 pulses are a result of the following processes:

adsorption of deuterium-containing species on the catalyst surface, incorporation and transfer of deuterium in the H/D pathways, and transport of desorbed deuterated species to the flow line. Variation of the flow rate allows adjustment of exposure time of the catalyst to the D_2 and C_2D_4 pulses to probe the relative rates of intermediates and the readsorption effect. The similarity in the decay of the transient responses in the dimensionless timescale and in the modeling of the deuterium transient response reveals that readsorption did not play a significant role in the transient responses of deuterated products.

The isotope effect on H_2/D_2 adsorption was manifested by a two-unequal-hump HD response to both the D_2 and C_2D_4 pulses. Deuterium from D_2 and C_2D_4 enters the reaction pathway to produce $C_2H_xD_{4-x}$ and $C_2H_xD_{6-x}$, probably through the Horiuti–Polanyi mechanism. These reaction steps involve intermediates with small τ and θ which are beyond the time resolution of our transient measurement. Deuterium enters the reaction pathway to form $C_2H_xD_{5-x}CDO$ through (i) H/D exchange with adsorbed acyl or enol and (ii) limited H/D exchange with adsorbed alkyl followed by CO insertion and deuteration. The former step has a small τ; the latter process involves several steps with a large τ that is comparable to that for the intermediate leading to $C_2H_5^{13}CHO$ from ^{13}CO pulse studies. The large τ reflects the slow reaction pathway whose products increase with increasing exposure time. *In situ* infrared studies trace the spillover of deuterium and identify the involvement of spillover deuterium in deuteration of adsorbed acyl species. Results of this study reveal the qualitative nature of hydrogenation/dehydrogenation pathways in ethylene hydrogenation and hydroformylation. Quantitative determination of the rate parameters for the reaction network for deuterated product formation cannot be achieved because of the inability to determine the composition of various deuterated isomers by MS. Quantification of τ and θ of intermediates for the lagging product responses can be achieved by compartment modeling of the intermediates. Determination of kinetic parameters for the rapid reaction has to rely on further improvement of time-resolution and sensitivity of transient approaches as well as FT-IR and MS instrumentation.

ACKNOWLEDGMENTS

The authors gratefully acknowledge the support of this research by the U.S. Department of Energy under Grant DG-FG-87PC79923 and partial support from the National Science Foundation under Grant CTS-942111996.

REFERENCES

1. Steinfeld, J., Francisco, J., and Hase, W., "Chemical Kinetics and Dynamics," Prentice–Hall, Englewood Cliffs, NJ, 1989.
2. Levine, R., and Bernstein, R., "Molecular Reaction Dynamics and Chemical Reactivity," Oxford Univ. Press, Oxford, 1987.
3. Ball, P., "Designing the Molecular World: Chemistry at the Frontier," Princeton Univ. Press, Princeton, NJ, 1994.
4. Tamaru, K., "Dynamic Heterogeneous Catalysis," Academic Press, New York, 1978.
5. Lay, T., Won, Y.-S., and Bozzelli, J. W., *Chem. Phys. Processes Combust.*, 357 (1995).
6. Tamaru, K., *in* "Catalysis: Science and Technology" (J. Anderson and M. Bourdart, Eds.), Springer-Verlag, Berlin, 1991.
7. Chuang, S. S. C., Balakos, M. W., Krishnamurthy, R., and Srinivas, G., *in* "Studies in Surface Science and Catalysis" (H. Curry-Hyde and R. Howe, Eds.), Vol. 81, Elsevier, New York, 1994.
8. Rabo, J., *in* "Proc. 10th Int. Cong. Catal., Part A" (L. Guczi, F. Solymosi, and P. Tetenyi, Eds.), Akad. Kiadó, Budapest, Hungary and Elsevier Science, Amsterdam, 1993.
9. Haller, G. L., and Coulston, G. W., *in* "Catalysis: Science and Technology" (J. R. Anderson and M. Bourdart, Eds.), Vol. 9, Springer-Verlag, New York, 1991.
10. Chuang, S. S. C., Brundage, M. A., Balakos, M. W., and Srinivas, G., *Appl. Spectrosc.* **49**(8), 1151 (1995).
11. Bileon, P., *J. Mol. Catal.* **21**, 17 (1983).
12. Shannon, S. L., and Goodwin, J. G., Jr., *Chem. Rev.* **95**, 677 (1995).
13. Chuang, S. S. C., and Pien, S., *J. Catal.* **135**, 618 (1992).
14. Chuang, S. S. C., Goodwin, J. G., Jr., and Wender, I., *J. Catal.* **92**, 416 (1985).
15. Balakos, M., and Chuang, S. S. C., *J. Catal.* **151**, 266 (1995).
16. Sachtler, W. M. H., and Ichikawa, M., *J. Phys. Chem.* **90**, 4752 (1986).
17. Brundage, M. A., and Chuang, S. S. C., *J. Catal.* **164**, 94 (1996).
18. Levenspiel, O., "Chemical Reaction Engineering," Wiley, New York, 1972.
19. Cremer, P., Su, X., Shen, Y., and Somorjai, G., *J. Am. Chem. Soc.* **118**, 2942 (1996).
20. Hair, M. L., "Infrared Spectroscopy in Surface Science," Decker, New York, 1967.
21. Conner, W. C., Jr., and Falconer, J. L., *Chem. Rev.* **95**, 759 (1995).
22. Fogler, H. S., "Elements of Chemical Reaction Engineering," Prentice–Hall, Englewood Cliffs, NJ, 1992.
23. Melander, L., and Saunders, W., "Reaction Rates of Isotopic Molecules," Wiley, New York, 1980.
24. White, M., "Heterogeneous Catalysis," Prentice–Hall, Englewood Cliffs, NJ, 1989.
25. Somorjai, G., *Chem. Rev.* **96**, 1223 (1996).
26. Cremer, P., McIntyre, B., and Salmeron, M., *Catal. Lett.* **34**, 11 (1995).
27. Horiuti, J., and Polanyi, M., *Trans. Faraday Soc.* **30**, 1164 (1934).
28. Horiuti, J., and Miyahara, K., "Hydrogenation of Ethylene on Metallic Catalysts, NBS-NSRDS No. 13," National Bureau of Standards, Washington, DC, 1968.
29. Brundage, M., and Chuang, S. S. C., *Catalysis Today*, Submitted for publication (1998).
30. Bond, G. C., "Catalysis by Metals," Academic Press, London, 1962.
31. Goddard, S., Cortright, R., and Dumesic, J., *J. Catal.* **137**, 186 (1992).
32. Kemball, C., *J. Chem. Soc.*, 756 (1956).
33. Mazanec, T., *J. Catal.* **98**, 115 (1986).
34. Takeuchi, A., and Katzer, J. R., *J. Phys. Chem.* **86**, 2438 (1982).
35. Brundage, M., Balakos, M., and Chuang, S. S. C., *J. Catal.*, in press (1998).